Comparing non-fullerene acceptors with fullerene in polymer solar cells: a case study with FTAZ and PyCNTAZ†

Nicole Bauer,[a] Qianqian Zhang,[a] Jingbo Zhao,[b] Long Ye,[c] Joo-Hyun Kim,[c] Iordania Constantinou,[d] Liang Yan,[a] Franky So,[d] Harald Ade,[c] He Yan[b] and Wei You*[a]

Non-fullerene acceptors (NFAs) are becoming a serious contender to fullerene-based electron acceptors in organic photovoltaics, due to their structural versatility and easily tunable optical and electronic properties. However, NFA-based solar cells often have a decreased short-circuit current (J_{sc}) and fill factor (FF) compared to their fullerene-based counterparts. Here, we investigate the fundamental causes of this decrease in the performance of solar cells using a non-fullerene acceptor (SF-PDI$_2$) paired with two polymer donors, FTAZ and PyCNTAZ, compared with their fullerene-based counterparts. Through a number of experimental techniques and morphological studies, we show that the SF-PDI$_2$-based solar cells suffer from insufficient charge generation, transport, and collection when compared with the PCBM-based solar cells. The SF-PDI$_2$-based solar cells show increased bimolecular recombination, which, together with other recombination loss mechanisms in these cells, causes a significant decrease in their J_{sc} and FF. Notably, the less pure domains, low electron mobility (on the order of 10^{-5} cm^2 V^{-1} s^{-1}), and imbalanced mobility (in regard to the hole mobility) further explain the low FF. On the other hand, the higher open-circuit voltage (V_{oc}) in the SF-PDI$_2$ devices is mainly due to the increase in the CT state energy. It is worth mentioning that the PyCNTAZ-based devices show an ultralow charge separation energy (ΔE_{CS}), close to 0 eV. Our results demonstrate that further increasing the mobility (both of electrons and holes) in these NFA-based solar cells would be a viable approach to further enhance the efficiency of these new types of solar cells, ideally, without losing the high V_{oc} of such cells.

Introduction

Organic photovoltaics (OPVs) are promising candidates for solar energy applications for reasons including the potentially low fabrication cost (from both a processing and a materials' perspective), light weight, and mechanical flexibility of the devices when compared to silicon solar cells. The most common electron acceptors used in OPVs are fullerene derivatives because of their high electron affinity and relatively high electron mobility.[1] Despite these advantages, fullerenes have a number of drawbacks, including difficult synthesis processes, rather fixed energy levels, and poor light absorption in the visible region. To address these fullerene-associated issues, non-fullerene acceptors (NFAs) have gained significant momentum in recent years, due to their many advantages over traditional fullerenes.[2] For example, one can easily tune the optical and electronic properties of NFAs *via* molecular designing, which could allow for enhanced open-circuit voltage (V_{oc}) from their energy levels matching those of the donor polymer[3,4] and increased current (J_{sc}) from their complementary absorption to that of the donor polymer.[5,6] Benefitting from the experiences gained and lessons learned from decades of research on fullerene-based bulk heterojunction (BHJ) systems, the community has made rapid progress in the past two years with record high efficiency reaching ∼12% for NFA-based devices,[7,8] on par with the highest efficiency achieved for fullerene blends.[9–11]

Though a higher V_{oc} is usually obtained for NFA-based organic solar cells than that of their fullerene-based counterparts, the NFA-based devices often suffer from a noticeably reduced short-circuit current (J_{sc}) and/or fill factor (FF).[12] Since both J_{sc} and FF are closely related to the loss mechanisms in photovoltaic devices (*e.g.*, bimolecular recombination),[13,14] it is important to understand such loss mechanisms in NFA-based solar cells, ideally in a comparative manner with the corresponding solar cells based on fullerenes. Unfortunately, such studies have only begun to emerge.[15,16]

[a]Department of Chemistry, University of North Carolina at Chapel Hill, Chapel Hill, North Carolina 27599, USA. E-mail: wyou@unc.edu

[b]Department of Chemistry, Hong Kong Branch of Chinese National Engineering Research Center for Tissue Restoration & Reconstruction, Hong Kong University of Science and Technology, Clear Water Bay, Kowloon, Hong Kong

[c]Department of Physics and ORaCEL, North Carolina State University, Raleigh, North Carolina 27695, USA

[d]Department of Materials Science and Engineering, North Carolina State University, Raleigh, North Carolina 27606, USA

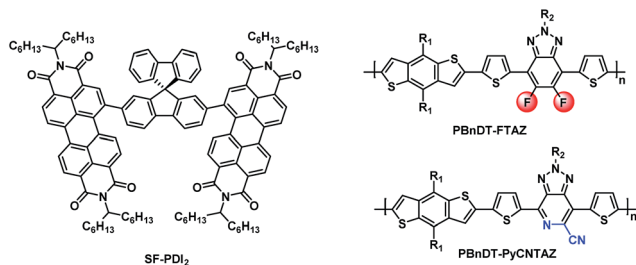† Electronic supplementary information (ESI) available. See DOI: 10.1039/c6ta10450a

Chart 1 Chemical structures of SF–PDI$_2$, FTAZ, and PyCNTAZ.

Fig. 1 (a) J–V characteristics of SF–PDI$_2$- and PCBM–based solar cells; (b) normalized absorption spectra of neat FTAZ, PyCNTAZ and SF–PDI$_2$ films.

We set our study by first choosing SF-PDI$_2$ as the small molecule, non-fullerene electron acceptor. In a previous study by Zhao *et al.*, SF-PDI$_2$ was paired with the polymer donor PffBT4T-2DT and achieved a high V_{oc} of 0.98 V in their BHJ devices, leading to a respectable power conversion efficiency (PCE) of 6.3%.[17] We then selected two TAZ-based donor polymers, FTAZ and PyCNTAZ (structures given in Chart 1), that have shown impressive device performance in their BHJ solar cells based on fullerene acceptors.[18,19] The first donor polymer, FTAZ, containing a fluorinated benzotriazole as the electron-accepting moiety, was reported by Price *et al.* in 2011.[18] They obtained a relatively high V_{oc} of 0.79 V with an impressive FF of 72%, giving an overall PCE of over 7%.[14,20] The other donor polymer chosen for this work, PyCNTAZ, was introduced by Li *et al.* in 2015.[19] In BHJ solar cells with PCBM, PyCNTAZ displayed a V_{oc} of 0.96 V, higher than that of FTAZ, leading to a higher PCE of 8.37% at an optimized active layer thickness of 300 nm.

In this study, we aim to directly compare the photovoltaic performance of four BHJ blends based on two acceptors (SF-PDI$_2$ and PC$_{61}$BM, referred to here as PCBM) and two donor polymers (FTAZ and PyCNTAZ), and investigate the device physics and morphology to determine the origins of the differences in performance. Notably, for both polymers, the SF-PDI$_2$-based photovoltaic device has a higher V_{oc} than the PCBM-based counterpart. This higher V_{oc} is directly correlated with the higher charge transfer state energy (E_{CT}) of the SF-PDI$_2$ blend, mainly due to the higher-lying lowest unoccupied molecular orbital (LUMO) level of SF-PDI$_2$. However, the SF-PDI$_2$-based device displays a lower FF than the PCBM-based device due to a mobility imbalance and less pure domains. Furthermore, the SF-PDI$_2$-based device shows a lower J_{sc}, which can be ascribed to inefficient charge transfer from the donor polymer to the non-fullerene acceptor (*i.e.*, SF-PDI$_2$) and increased non-geminate recombination in such non-fullerene acceptor-based blends.

Results and discussion

Photovoltaic performance

To investigate the performance differences displayed between devices containing a fullerene and a non-fullerene acceptor, the small molecule acceptor SF-PDI$_2$ was paired with the donor polymers FTAZ and PyCNTAZ in bulk heterojunction (BHJ) solar cells. Devices were also fabricated using PCBM as the acceptor with both polymers for comparison. A conventional device
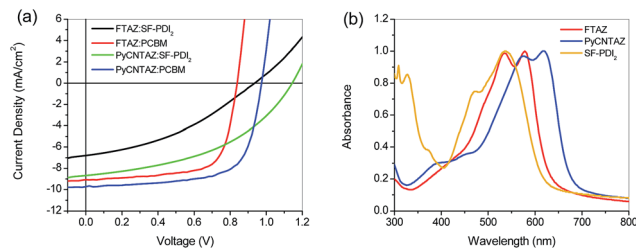
Table 1 Photovoltaic characteristics of SF–PDI$_2$- and PCBM–based solar cells

Blend	J_{sc} (mA cm^{-2})	V_{oc} (V)	FF (%)	PCE (%)
FTAZ:SF-PDI$_2$	6.70 ± 0.29	0.935 ± 0.005	36.7 ± 1.6	2.30 ± 0.15
FTAZ:PCBM	9.16 ± 0.32	0.846 ± 0.007	73.3 ± 2.0	5.68 ± 0.23
PyCNTAZ:SF-PDI$_2$	8.15 ± 0.12	1.152 ± 0.003	46.5 ± 1.3	4.37 ± 0.17
PyCNTAZ:PCBM	10.10 ± 0.38	0.975 ± 0.003	64.8 ± 2.3	6.39 ± 0.41

configuration was used (ITO/HTL/active layer/Ca/Al), where the hole transport layer (HTL) was poly(3,4-ethylenedioxythiophene)-poly(styrenesulfonate) (PEDOT:PSS) for FTAZ-based devices and copper thiocyanate (CuSCN) for PyCNTAZ-based devices. Due to the deeper HOMO (highest occupied molecular orbital) level of PyCNTAZ, using CuSCN as the HTL can help improve the photovoltaic device performance when compared to PEDOT:PSS as the HTL, as we previously demonstrated.[19] Active layer thicknesses for all four devices were kept at ~150 nm to minimize thickness effects on performance, and the donor : acceptor (D : A) ratio in the BHJ blend for all devices was 1 : 2 by weight. The J–V curves are shown in Fig. 1a and the photovoltaic characteristics are summarized in Table 1. For the SF-PDI$_2$ blends, the PyCNTAZ-based device displays a higher J_{sc} than the FTAZ-based device, which can be ascribed to less overlapping/more complementary absorption of PyCNTAZ and SF-PDI$_2$ (Fig. 1b) and efficient utilization of both components to generate current. Pleasingly, when compared to the fullerene-based device, the SF-PDI$_2$-based device gives a higher V_{oc} value for both polymers than the PCBM-based one, *i.e.*, 0.935 V *vs.* 0.846 V for FTAZ:SF-PDI$_2$ and FTAZ:PCBM, respectively, and 1.152 V *vs.* 0.975 V for PyCNTAZ:SF-PDI$_2$ and PyCNTAZ:PCBM, respectively. However, the SF-PDI$_2$-based device has a lower J_{sc} and FF than the PCBM-based device, leading to a lower power conversion efficiency (PCE) by the former device for both polymers. Below, we will discuss each device characteristic in further detail and strive to identify the underlying reasons for the observed trends.

Open circuit voltage (V_{oc})

To determine the cause of the higher V_{oc} for SF-PDI$_2$-based devices, we first considered the energy levels of the donors
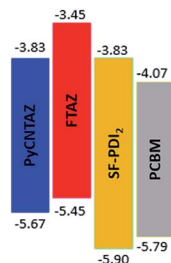
Fig. 2 HOMO and LUMO levels of PyCNTAZ, FTAZ, SF–PDI$_2$, and PCBM.

and acceptors. Such values can be extracted from previous reports,[17–19,21] which are presented in Fig. 2. It has long been argued that V_{oc} is primarily proportional to the difference between the LUMO energy level of the acceptor and the HOMO energy level of the donor, if ohmic contacts are achieved at both cathode and anode interfaces. SF-PDI$_2$ has a higher-lying LUMO level than PCBM, -3.83 eV compared to -4.07 eV, respectively. This difference (~0.2 eV) certainly accounts for a higher V_{oc} for both SF-PDI$_2$-based solar cells; yet the observed V_{oc} difference (~0.09 V for FTAZ-based devices and ~0.15 V for PyCNTAZ-based devices) needs further investigation (*vide infra*).

Vandewal *et al.* demonstrated that V_{oc} is primarily determined by the interfacial charge-transfer (CT) states between the donor and the acceptor, with additional loss coming from the radiative emission and non-radiative emission.[22,23] Eqn (1) presents the relationship,

$$V_{oc} = \frac{kT}{q}\ln\left(\frac{J_{ph}}{J_0} + 1\right)$$
$$= \frac{E_{CT}}{q} + \frac{kT}{q}\ln\left(\frac{J_{sc}h^3c^2}{fq2\pi(E_{CT} - \lambda)}\right) + \frac{kT}{q}\ln(\text{EQE}_{EL}) \quad (1)$$

which can also be re-written as (q is the elementary charge, *i.e.*, e)

$$eV_{oc} = E_{CT} + kT\ln\left(\frac{J_{sc}h^3c^2}{fq2\pi(E_{CT} - \lambda)}\right) + kT\ln(\text{EQE}_{EL}) \quad (2)$$

According to Faist *et al.*,[24] the energy difference between eV_{oc} and E_{CT} is the loss due to the non-geminate recombination (*i.e.*, $\Delta E_{NG} = E_{CT} - eV_{oc}$), and the charge separation energy/exciton splitting energy ($\Delta E_{CS} = E_{opt} - E_{CT}$) is the difference between

the optical gap (E_{opt}) and the energy of the CT state manifold. Unlike a typical inorganic solar cell where there are essentially no CT states (thus $\Delta E_{CS} \sim 0$), the presence of the CT state manifold constructs a significant channel of energy loss (ΔE_{CS}), manifested by the typically observed smaller V_{oc} when compared with the band gap (*i.e.*, $eV_{oc} = E_{opt} - \Delta E_{CS} - \Delta E_{NG}$). Experimentally, high sensitivity external quantum efficiency (EQE) measurements were performed and the resulting spectra (Fig. 3) were fitted to obtain an estimate for E_{CT} (Table 2) using eqn (3).[21]

$$\text{EQE}(E) \propto \frac{1}{E\sqrt{4\pi\lambda kT}}\exp\left(-\frac{(E_{CT} + \lambda - E)^2}{4\lambda kT}\right) \quad (3)$$

With the optically determined band gap (E_{opt}) and measured V_{oc}, the aforementioned ΔE_{CS} and ΔE_{NG} can thereby be determined for each blend (Table 2).

For both polymers, the difference in E_{CT} between the fullerene and the non-fullerene device is almost identical to the difference in V_{oc} (numerically), for example, a ΔE_{CT} of 0.15 eV (1.55–1.39) *vs.* a ΔV_{oc} of 0.16 (0.93–0.77) for FTAZ. This observation implies that the V_{oc} loss in these systems is independent of the choice of acceptor (*i.e.*, SF-PDI$_2$ or PCBM). Furthermore, ΔE_{NG} is similar for all devices at ~0.6 eV, indicating that V_{oc} losses from non-geminate recombination are also very similar in all four blends. However, while the charge separation energy (ΔE_{CS}) for FTAZ-based cells is 'normal', 0.27 eV for FTAZ:PCBM and 0.44 eV for FTAZ:SF-PDI$_2$, the PyCNTAZ-based devices display an exceptionally low driving force (ΔE_{CS}) of ~0.03 eV for both devices. While not as common, devices that maintain efficient charge separation and high performance but display a low ΔE_{CS} have been recently reported, interestingly, also for SF-PDI$_2$-based devices.[25] This exciting discovery certainly warrants further investigation, since achieving a low ΔE_{CS} is a very promising approach to further enhance the efficiency of polymer solar cells.

Short circuit current (J_{sc})

Comparing the J_{sc} values in Table 1 raises one important question we try to answer with this study: why is J_{sc} lower in both cases for SF-PDI$_2$-based devices when compared with PCBM-based devices? In fact, there are multiple possible causes which can occur at various stages of the photovoltaic process (*i.e.*, charge generation, charge transport and charge collection), to account for a lowered J_{sc}. For example, insufficient exciton quenching could lead to insufficient charge generation, and bimolecular recombination could compete with charge transport to the electrode, to name a few.

We first measured the photoluminescence (PL) quenching to study exciton splitting/charge generation in the BHJ blends, and the data are presented in Fig. 4. Due to the absorption overlap of SF-PDI$_2$ with the two donor polymers, we chose to use D : A = 10 : 1 to allow for quantitative determination of PL quenching (PL quenching with D : A = 1 : 2 in Fig. S3†). It is clear from the results that SF-PDI$_2$-based blends show less PL quenching than PCBM-based blends (for both FTAZ and PyCNTAZ), indicating
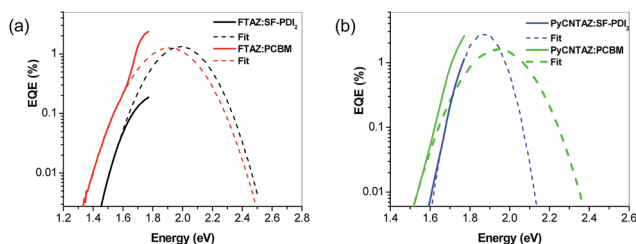

Fig. 3 Measured low energy external quantum efficiency (EQE) curves and calculated fittings of (a) FTAZ and (b) PyCNTAZ based solar cells.

Table 2 V_{oc}, E_{CT}, and energy losses of FTAZ- and PyCNTAZ-based solar cells

Blend	V_{oc}[b] (V)	E_{opt} (eV)	E_{CT} (eV)	ΔE_{loss} (eV) $E_{opt} - eV_{oc}$	ΔE_{CS} (eV) $E_{opt} - E_{CT}$	ΔE_{NG} (eV) $E_{CT} - eV_{oc}$
FTAZ:SF-PDI$_2$	0.93	1.99	1.55	1.06	0.44	0.62
FTAZ:PCBM	0.77	1.66[a]	1.39	0.89	0.27	0.62
PyCNTAZ:SF-PDI$_2$	1.10	1.80	1.76	0.70	0.04	0.66
PyCNTAZ:PCBM	0.97	1.66[a]	1.63	0.69	0.03	0.66

[a] Please note that the band gap of PCBM was used here as the band gap of the polymer is larger than the band gap of PCBM. [b] The top contacts for these devices (LiF/Al) were evaporated at NCSU after spin casting the active layer at UNC.

that there may be an issue with donor to acceptor charge transfer in the SF-PDI$_2$-based systems, especially for PyCNTAZ. Incomplete charge transfer in the device would decrease the J_{sc} at the source of charge generation. For the FTAZ-based blends (Fig. 4a), the amount of quenching was 82% and 96% for FTAZ:SF-PDI$_2$ and FTAZ:PCBM, respectively, suggesting that the driving force ($\Delta E_{CS} > 0.2$ eV) is large enough to allow only 10% acceptor to sufficiently quench the PL of FTAZ with either SF-PDI$_2$ or PCBM. On the other hand, for PyCNTAZ-based blends (Fig. 4b), the amount of quenching was only 34% and 81% for PyCNTAZ:SF-PDI$_2$ and PyCNTAZ:PCBM, respectively. It is possible that due to the low driving force ($\Delta E_{CS} \sim 0$ eV) of the PyCNTAZ blends, energy transfer may also play an important role in the PL quenching, in addition to photo-induced charge transfer. In the PyCNTAZ:PCBM blend, though the driving force is small ($\Delta E_{CS} \sim 0$ eV), PCBM has a smaller band gap and there can be both energy transfer and charge transfer in the PyCN-TAZ:PCBM system. Thus, ~10% PCBM is still able to quench a much larger degree of the PL of PyCNTAZ (Fig. 4b). However, in the PyCNTAZ:SF-PDI$_2$ blend, there is essentially no energy transfer for quenching the PL of PyCNTAZ because the band gap of SF-PDI$_2$ is larger than that of PyCNTAZ; thus, the PL quenching is purely dependent upon the photo-induced charge transfer for the PyCNTAZ:SF-PDI$_2$ blend, which is not sufficient due to the low driving force ($\Delta E_{CS} \sim 0$ eV).

We next attempted to probe the recombination mechanisms occurring in these devices, since the recombination, in particular the bimolecular recombination, is known to have a strong impact on charge transport. To this end, light intensity dependence of J_{sc} and V_{oc} was measured for the four devices. On the one hand, J_{sc} is known to have a power law dependence on light intensity, following the relationship

$$J_{sc} \propto I^{\alpha} \tag{4}$$

where I is the light intensity and α is the slope of the log–log plot of J_{sc} vs. intensity.[26] An α value close to unity is indicative of weak bimolecular recombination under short-circuit conditions. The log plot of J_{sc} vs. light intensity is displayed in Fig. 5a. For both polymers, the α value for the fullerene-based device is closer to one than that of the non-fullerene device, suggesting increased bimolecular recombination in the SF-PDI$_2$-based devices at short circuit. The increased recombination would compete with charge extraction and lead to a lower current in the non-fullerene based devices.

On the other hand, when bimolecular recombination is the only loss mechanism, V_{oc} can be related to light intensity by the following equation:

$$V_{oc} = \frac{E_{gap}}{q} - \frac{kT}{q} \ln\left[\frac{(1 - P_D)\gamma N_c^2}{P_D G}\right] \tag{5}$$

where E_{gap} is the HOMO$_{donor}$ − LUMO$_{acceptor}$ difference, k is the Boltzmann constant, T is the temperature in Kelvin, q is the elementary charge (i.e., e), P_D is the dissociation probability of electron–hole pairs, γ is the recombination constant, N_C is the effective density of states, and G is the generation rate of bound electron–hole pairs.[26] In this equation, G is proportional to the light intensity, and a semi-log plot of V_{oc} vs. light intensity will yield a slope of kT/q if bimolecular recombination is the sole loss mechanism. Fig. 5b presents the V_{oc} vs. light intensity data for all four devices. For both polymers, the PCBM-based blends have a slope very close to kT/q, indicating that bimolecular recombination is the major loss mechanism under open-circuit conditions in these devices. However, the FTAZ:SF-PDI$_2$ device shows a slope greater than kT/q whereas PyCNTAZ:SF-PDI$_2$ has a slope less than kT/q. These results indicate that the FTAZ:SF-
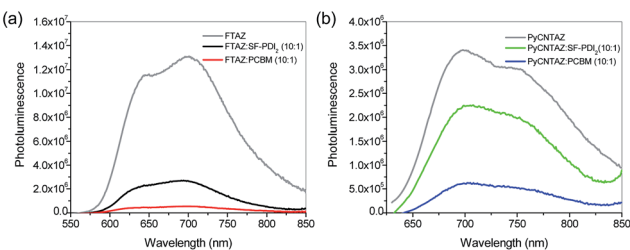
Fig. 4 Photoluminescence of neat (a) FTAZ (excitation at 532 nm) and (b) PyCNTAZ (excitation at 618 nm) films and the blend films with SF-PDI$_2$ and PCBM (D : A = 10 : 1).
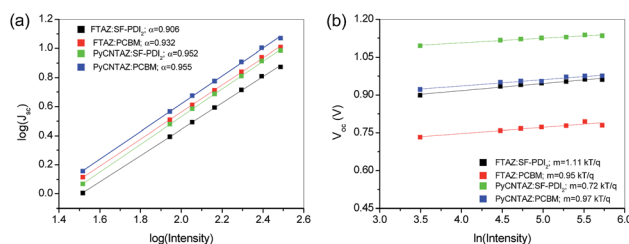
Fig. 5 Light intensity dependence of (a) short-circuit current and (b) open-circuit voltage.

PDI$_2$ device suffers from a combination of trap-assisted and bimolecular recombination under open-circuit conditions,[27,28] while PyCNTAZ:SF-PDI$_2$ is mainly affected by surface recombination.[29,30] Due to these additional recombination channels, the number of charges that can successfully traverse the active layer and make it to the electrode will be less for the SF-PDI$_2$-based devices compared to the PCBM-based ones, which would decrease the current.

Finally, we studied the charge collection by comparing the charge collection probability, $P(E,T)$, for all blends. Experimentally, the photocurrent density (J_{ph}) was first measured as a function of the effective voltage V_{eff} (Fig. 6a) for each device. J_{ph} is defined as $J_L - J_D$, where J_L is the current density under illumination and J_D is the current density in the dark, and V_{eff} is $V_0 - V$, where V_0 is the voltage at which $J_{ph} = 0$.[31,32] The photocurrent density (J_{ph}) was then used to calculate the charge collection probability, $P(E,T)$, for each blend using the equation

$$P(E,T) = \frac{J_{ph}}{J_{ph,sat}} \qquad (6)$$

where $J_{ph,sat}$ is the saturation photocurrent density of the device.[32] Under short-circuit conditions, the PCBM-based devices have a higher $P(E,T)$ than the non-fullerene devices, 92.4% compared to 73.5% for FTAZ:PCBM and FTAZ:SF-PDI$_2$, respectively, and 89.3% compared to 79.8% for PyCNTAZ:PCBM and PyCNTAZ:SF-PDI$_2$, respectively. These results indicate that the charge collection process is more efficient in the fullerene devices, which contributes to the higher J_{sc} of the fullerene-based devices for both polymers.

Fill factor (FF)

We previously showed that the main reason for the unusually high FF of the FTAZ:PCBM device was the high hole mobility (1.2×10^{-3} cm^2 V^{-1} s^{-1}) and the balanced mobility (i.e., electron mobility on the same order of magnitude, $\sim 5 \times 10^{-3}$ cm^2 V^{-1} s^{-1}).[14] Indeed, the space-charge limited current (SCLC) mobilities of the PCBM-based devices in this study further confirmed the balanced mobilities (Table 3) for both polymers.

However, when switching out PCBM for SF-PDI$_2$, the SF-PDI$_2$-based devices show a large imbalance in the electron and the hole mobility for both polymers (Table 3). Proctor et al. have previously shown that low and imbalanced mobilities can reduce the fill factor of a solar cell.[33] In our case, the hole mobility of the non-fullerene devices is one order of magnitude
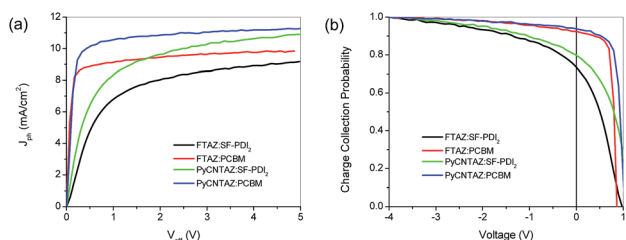
Table 3 Electron and hole mobilities of SF-PDI$_2$- and PCBM-based solar cells

Blend	Electron mobility ($\times 10^{-3}$ cm^2 V^{-1} s^{-1})	Hole mobility ($\times 10^{-3}$ cm^2 V^{-1} s^{-1})
FTAZ:SF-PDI$_2$	0.0368 ± 0.007	0.635 ± 0.219
FTAZ:PCBM	1.68 ± 0.565	4.23 ± 3.33
PyCNTAZ:SF-PDI$_2$	0.019 ± 0.003	0.504 ± 0.136
PyCNTAZ:PCBM	2.28 ± 1.43	1.26 ± 0.515

larger than the electron mobility; this large mobility imbalance is likely a major cause of the decreased FF in the SF-PDI$_2$-based devices.

In addition to the mobility imbalance, the SF-PDI$_2$-based devices also display lower mobilities overall, in particular, for electrons (on the order of 10^{-5} cm^2 V^{-1} s^{-1}). This may be due to the morphology of the SF-PDI$_2$-based films, which will be discussed in more detail in the next section. The low, imbalanced mobilities can lead to a build-up of space charge and exacerbate the charge transport via increased bimolecular recombination. This agrees with the results of the light intensity measurements, which indicate that the SF-PDI$_2$-based devices suffer from more recombination than the PCBM-based devices. The increased recombination would not only decrease the J_{sc} as mentioned previously, but also have a negative effect on the FF for the non-fullerene based devices.

Morphology

The morphology of BHJ thin films offers important information to further understand the observed photovoltaic behavior of these thin film based devices. To determine the molecular packing within the neat and blend films, grazing incidence wide-angle X-ray scattering (GIWAXS) measurements were performed. The scattering signatures of neat FTAZ and PyCNTAZ films are very similar, and both exhibit clear (100) peaks at $q = 0.3$ Å^{-1} in the in-plane direction and (010) peaks located at $q = 1.7$ Å^{-1} in the out-of-plane direction (Fig. 7a and b), suggesting that the polymers have a face-on orientation with respect to the substrate. Such a face-on feature was frequently observed before in many high-performance conjugated polymers and considered to be advantageous for hole transport across the active layer.[34] As shown in Fig. 7c, the neat SF-PDI$_2$ film does not display a (010) reflection peak; rather, it shows weak (100) diffuse rings and an amorphous halo around $q = 1.3$ Å^{-1} without a clear orientation preference.

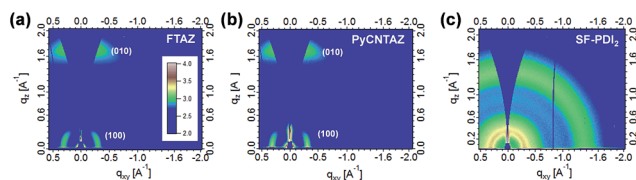**Fig. 6** (a) Photocurrent density and (b) charge collection probability ($P(E,T)$) of SF-PDI$_2$- and PCBM-based solar cells.

Fig. 7 GIWAXS 2D patterns of the thin films based on neat materials: (a) FTAZ; (b) PyCNTAZ; (c) SF-PDI$_2$.
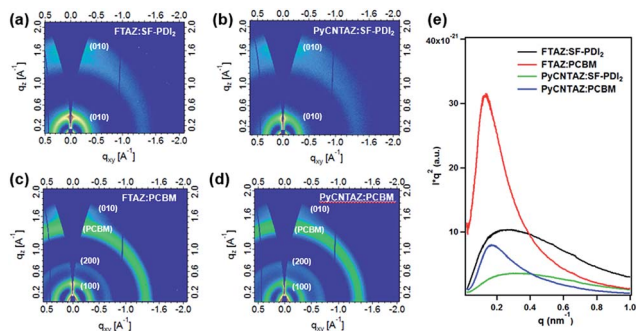
Fig. 8 GIWAXS 2D patterns of (a) FTAZ:SF-PDI$_2$, (b) FTAZ:PCBM, (c) PyCNTAZ:SF-PDI$_2$ and (d) PyCNTAZ:PCBM blend films; (e) Lorentz-corrected and thickness- and contrast-normalized circular averaged R-SoXS profiles of the blend films acquired at 283.2 eV to optimize the polymer:acceptor contrast over the mass thickness contrast.

Shown in Fig. 8a–d are the 2D GIWAXS patterns of these polymers blended with PCBM or SF-PDI$_2$. The SF-PDI$_2$-based blend films display weak (100) and (010) diffraction peaks, indicative of poor lamellar packing and π–π stacking. In contrast, the PCBM-based blends exhibit more clear lamellar (100) and (200) peaks, and a (010) peak in the out-of-plane direction in addition to an isotropic ring located at $q = 1.35$ Å^{-1}, which is originated from pure PCBM aggregates.[35] Comparison of the GIWAXS patterns between fullerene and SF-PDI$_2$-based films indicates that the PCBM-based films are more ordered, which agrees well with the higher hole/electron mobility observed for these PCBM-based devices (Table 3). A higher degree of molecular ordering in the film could afford improved charge transport and thus higher charge mobility, leading to the higher J_{sc} and FF values measured for the PCBM-based devices.

Resonant soft X-ray scattering (R-SoXS) was also utilized to determine the domain spacing and relative average composition variation (ACV) of the four blend films. The Lorentz corrected R-SoXS profiles acquired at a photon energy of 283.2 eV are normalized for thickness, contrast, and absorption differences (Fig. 8e).[36] All R-SoXS profiles are dominated by a single size distribution and the relative ACV can be extracted via integration of the scattering profiles over the full q-range probed and normalized to the highest ACV assigned a value of 1 (Table 4). The relative ACVs are 0.83 and 1 for FTAZ:SF-PDI$_2$ and FTAZ:PCBM, respectively, and 0.49 and 0.56 for PyCNTAZ:SF-PDI$_2$ and PyCNTAZ:PCBM, respectively. Generally, a higher relative ACV (i.e., more pure domains) is important as impure

domains lead to enhanced biomolecular recombination and thus lower device FF in both fullerene and non-fullerene based OPV systems.[37,38] In our case study, the highest relative ACV obtained in the FTAZ:PCBM film is quite consistent with its highest device FF up to ∼73%. It is clear that the PCBM blends have more pure domains for both polymers, which is another factor contributing to the higher FF of the fullerene devices. The long period (domain spacing) of the SF-PDI$_2$ films is close to the exciton diffusion length, 25.6 nm for FTAZ:SF-PDI$_2$ and 20.0 nm for PyCNTAZ:SF-PDI$_2$. Despite having a longer long period (49.0 nm for FTAZ:PCBM and 37.7 nm for PyCNTAZ:PCBM), the PCBM-based devices display higher J_{sc} and FF values, likely due in part to the higher charge mobility of these PCBM-based systems, which allows for more efficient charge transport and extraction. As shown in the 12%-efficiency NFA-based devices,[38,39] the blend films based on IT-M are more ordered compared with the SF-PDI$_2$ films. We thus speculate that applying other NFAs with higher crystallinity may be the key to overcoming the current limitations and further boosting the efficiency of non-fullerene devices based on FTAZ and PyCNTAZ polymers.

Conclusions

Solar cells based on the non-fullerene acceptor SF-PDI$_2$ have a larger V_{oc} than those based on PCBM; however, they also have a lower J_{sc} and FF, leading to a decreased overall power conversion efficiency. The increased V_{oc} in the non-fullerene devices is explained by the higher-lying LUMO level of SF-PDI$_2$, which increases the HOMO$_{donor}$ − LUMO$_{acceptor}$ gap, and more importantly, leads to a higher E_{CT} for these devices. In all four devices, the energy loss due to non-geminate recombination (ΔE_{NG}) is very similar (∼0.6 eV), yet the driving force for charge separation (ΔE_{CS}) is exceptionally small (∼0.03 eV) for the PyCNTAZ-based devices (with either PCBM or SF-PDI$_2$ as the acceptor). This interesting discovery certainly warrants further investigation. For example, what structural features of molecules would lead to such a low ΔE_{CS}? On the other hand, the SF-PDI$_2$-based devices show insufficient charge generation, transport and collection, which would explain the low J_{sc} of these devices. Notably, the light intensity dependence of V_{oc} and J_{sc} indicates more recombination loss channels, including trap-assisted recombination and surface recombination in the SF-PDI$_2$-based devices, in addition to the already increased bimolecular recombination loss in these devices. All these recombination losses would account for the decreased J_{sc} of the SF-PDI$_2$-based solar cells. Finally, the SF-PDI$_2$-based devices demonstrate less pure domains, low electron mobilities, and an imbalance in the electron and hole mobilities, all of which contribute to the observed decrease in the FF.

In summary, our understanding of the causes of the decreased J_{sc} and FF generally observed in non-fullerene acceptor based OPVs can aid in the designing of new non-fullerene acceptors with improved J_{sc} and FF, while maintaining the potential increase in V_{oc} in these non-fullerene acceptor based solar cells.

Table 4 Domain characteristics of the four blend films extracted from the R-SoXS measurements

Blend	Relative ACV	Long period [nm]
FTAZ:SF-PDI$_2$	0.83	25.6
FTAZ:PCBM	1	49.0
PyCNTAZ:SF-PDI$_2$	0.49	20.0
PyCNTAZ:PCBM	0.56	37.7

Experimental

Synthesis

FTAZ,[18] PyCNTAZ,[19] and SF-PDI$_2$ [17] were synthesized according to a literature procedure. The purity of all synthesized molecular materials was confirmed by NMR analysis.

Device fabrication

Solar cells were fabricated on glass substrates with patterned indium doped tin oxide (ITO). The ITO substrates were sonicated in deionized water, acetone, and isopropyl alcohol for fifteen minutes each, followed by UV-ozone treatment for 15 minutes. For FTAZ devices, PEDOT:PSS (Clevios PH500 from Heraeus) was spin cast onto the cleaned ITO at 4000 rpm for 60 s, and then baked at 130 °C for fifteen minutes in air. The substrates were then transferred into a nitrogen filled glovebox. For PyCNTAZ devices, CuSCN was dissolved in dipropylsulfide (20 mg mL^{-1}) and stirred for 24 h, after which the saturated solution was filtered with a 0.2 μm poly(tetrafluoroethylene) (PTFE) filter. CuSCN was spin cast onto the cleaned ITO substrate at 1000 rpm for 60 s, and then baked at 80 °C for 15 min in a glovebox under a nitrogen atmosphere. Donor : acceptor blend solutions were prepared (D : A = 1 : 2, 7 mg mL^{-1} polymer for all four solutions) in 1,2,4-trichlorobenzene and stirred at 130 °C for 5 h. The solutions were spin cast onto the PEDOT:PSS or CuSCN films for 60 s at an appropriate speed and then dried under vacuum to yield ∼150 nm films. The devices were finished by evaporation of 30 nm of calcium and 70 nm of aluminum as the cathode and tested under AM 1.5G irradiation calibrated with an NREL certified standard silicon solar cell. Current density–voltage curves were measured *via* a Keithley 2400 digital source meter.

SCLC measurements

Electron and hole mobilities were measured *via* the space-charge limited current (SCLC) method. Electron-only devices were fabricated with the configuration ITO/PEI/donor:acceptor/Ca/Al, where PEI is polyethyleneimine, used for reducing the work function of ITO.[40] Hole-only devices were fabricated with the configuration ITO/HTL/donor:acceptor/MoO$_3$/Al, where the HTL was PEDOT:PSS for FTAZ-based devices and CuSCN for PyCNTAZ-based devices. The dark current densities were measured with an applied voltage from 0 to 6 V using a Keithley 2400 digital source meter. The applied voltage was corrected from the voltage drop due to series and contact resistance. The Mott–Gurneys law was utilized to extract the mobility values:

$$J = \frac{9}{8}\varepsilon_r \varepsilon_0 \mu_h \frac{V^2}{L^3}$$

where ε_r is the dielectric constant of the polymer, ε_0 is the permittivity of free space, μ_h is the hole mobility, V is the voltage drop across the device, and L is the thickness of the active layer.

Long wavelength EQE measurements

Devices for long wavelength EQE measurements were spin cast at the University of North Carolina Chapel Hill, and the top contacts were evaporated at North Carolina State University.

Active layer thicknesses were ∼150 nm for both FTAZ devices and ∼120 nm for PyCNTAZ devices. Long wavelength EQE measurements were conducted using an in-house setup consisting of a xenon DC arc lamp, an ORIEL 74125 monochromator, a Keithley 428 current amplifier, an SR 540 chopper system and a Stanford Research Systems SR830 DSP lock-in amplifier. For the calibration of the spectrum, a Si and a Ge photodiode purchased from Newport Corporation were used as necessary. 700 nm and 1000 nm long-pass filters were used in order to isolate the desired part of the spectrum for the monitoring of the sub-bandgap response.

Morphology

GIWAXS, R-SoXS and NEXAFS reference spectra measurements were respectively performed at the beamline 7.3.3 [41], beamline 11.0.1.2,[42] and beamline 5.3.2.2,[43] Advanced Light Source (ALS), Lawrence Berkeley National Laboratory, following the previously established protocols. GIWAXS data were acquired just above the critical angle (0.13°) of the films with a hard X-ray energy of 10 keV, and silver behenate (AgB) was used for geometry calibration. R-SoXS was performed in a transmission geometry with linearly polarized photons under high vacuum (1 × 10^{-7} Torr) and a cooled (−45 °C) CCD (Princeton PI-MTE, 2048 pixels × 2048 pixels) was used to capture the soft X-ray scattering 2D maps and a PS300 was used for geometry calibration. The raw 2D X-ray data were processed with a modified version of NIKA into 1D scattering profiles $I(q)$.[44]

Acknowledgements

Notes and references

1 Y. He and Y. Li, *Phys. Chem. Chem. Phys.*, 2011, **13**(6), 1970–1983.

2 S. Li, Z. Zhang, M. Shi, C.-Z. Li and H. Chen, *Phys. Chem. Chem. Phys.*, 2017, **19**, 3440–3458.

3 Y. Lin, F. Zhao, Q. He, L. Huo, Y. Wu, T. C. Parker, W. Ma, Y. Sun, C. Wang, D. Zhu, A. J. Heeger, S. R. Marder and X. Zhan, *J. Am. Chem. Soc.*, 2016, **138**(4), 4955–4961.

4 T. Liu, D. Meng, Y. Cai, X. Sun, Y. Li, L. Huo, F. Liu, Z. Wang, T. P. Russell and Y. Sun, *Adv. Sci.*, 2016, **3**, 1600117.

5 H. Yao, Y. Chen, Y. Qin, R. Yu, Y. Cui, B. Yang, S. Li, K. Zhang and J. Hou, *Adv. Mater.*, 2016, 1–5.

6 L. Gao, Z. Zhang, H. Bin, L. Xue, Y. Yang, C. Wang, F. Liu, T. P. Russell and Y. Li, *Adv. Mater.*, 2016, 1–8.

7 W. Zhao, D. Qian, S. Zhang, S. Li, O. Inganäs, F. Gao and J. Hou, *Adv. Mater.*, 2016, **28**(23), 4734–4739.

8 S. Li, L. Ye, W. Zhao, S. Zhang, S. Mukherjee, H. Ade and J. Hou, *Adv. Mater.*, 2016, **28**, 9423–9429.

9 Z. He, B. Xiao, F. Liu, H. Wu, Y. Yang, S. Xiao, C. Wang, T. P. Russell and Y. Cao, *Nat. Photonics*, 2015, **9**(3), 174–179.

10 V. Vohra, K. Kawashima, T. Kakara, T. Koganezawa, I. Osaka, K. Takimiya and H. Murata, *Nat. Photonics*, 2015, **9**, 403–409.

11 J. Zhao, Y. Li, G. Yang, K. Jiang, H. Lin, H. Ade, W. Ma and H. Yan, *Nat. Energy*, 2016, **1**(2), 15027.

12 Y. Lin and X. Zhan, *Mater. Horiz.*, 2014, **1**(5), 470–488.

13 G. Lakhwani, A. Rao and R. H. Friend, *Annu. Rev. Phys. Chem.*, 2014, **65**(1), 557–581.

14 W. Li, S. Albrecht, L. Yang, S. Roland, J. R. Tumbleston, T. McAfee, L. Yan, M. A. Kelly, H. Ade, D. Neher and W. You, *J. Am. Chem. Soc.*, 2014, **136**(44), 15566–15576.

15 Y. Lin, P. Cheng, Y. Li and X. Zhan, *Chem. Commun.*, 2012, **48**(39), 4773.

16 D. Meng, D. Sun, C. Zhong, T. Liu, B. Fan, L. Huo, Y. Li, W. Jiang, H. Choi, T. Kim, J. Y. Kim, Y. Sun, Z. Wang and A. J. Heeger, *J. Am. Chem. Soc.*, 2016, **138**(1), 375–380.

17 J. Zhao, Y. Li, H. Lin, Y. Liu, K. Jiang, C. Mu, T. Ma, J. Y. Lin Lai, H. Hu, D. Yu and H. Yan, *Energy Environ. Sci.*, 2015, **8**(2), 520–525.

18 S. C. Price, A. C. Stuart, L. G. Yang, H. X. Zhou and W. You, *J. Am. Chem. Soc.*, 2011, **133**, 4625–4631.

19 W. Li, L. Yan, H. Zhou and W. You, *Chem. Mater.*, 2015, **27**(18), 6470–6476.

20 W. Li, L. Yang, J. R. Tumbleston, L. Yan, H. Ade and W. You, *Adv. Mater.*, 2014, **26**(26), 4456–4462.

21 E. T. Hoke, K. Vandewal, J. A. Bartelt, W. R. Mateker, J. D. Douglas, R. Noriega, K. R. Graham, J. M. J. Fréchet, A. Salleo and M. D. Mcgehee, *Adv. Energy Mater.*, 2013, **3**(2), 220–230.

22 K. Vandewal, K. Tvingstedt, A. Gadisa, O. Inganäs and J. V. Manca, *Nat. Mater.*, 2009, **8**, 904–909.

23 K. Vandewal, K. Tvingstedt, A. Gadisa, O. Inganäs and J. V. Manca, *Phys. Rev. B: Condens. Matter Mater. Phys.*, 2010, **81**(12), 125204.

24 M. A. Faist, T. Kirchartz, W. Gong, R. S. Ashraf, I. Mcculloch, J. C. De Mello, N. J. Ekins-Daukes, D. D. C. Bradley and J. Nelson, *J. Am. Chem. Soc.*, 2011, **134**(1), 685–692.

25 J. Liu, S. Chen, D. Qian, B. Gautam, G. Yang, J. Zhao, J. Bergqvist, F. Zhang, W. Ma, H. Ade, O. Inganäs, K. Gundogdu, F. Gao and H. Yan, *Nat. Energy*, 2016, **1**(9), 16089.

26 A. K. K. Kyaw, D. H. Wang, V. Gupta, W. L. Leong, L. Ke, G. C. Bazan and A. J. Heeger, *ACS Nano*, 2013, (5), 4569–4577.

27 L. Lu, T. Zheng, T. Xu, D. Zhao and L. Yu, *Chem. Mater.*, 2015, **27**(2), 537–543.

28 S. R. Cowan, A. Roy and A. J. Heeger, *Phys. Rev. B: Condens. Matter Mater. Phys.*, 2010, **82**(24), 245207.

29 V. V. Brus, *Org. Electron.*, 2016, **29**, 1–6.

30 S. Solak, P. W. M. Blom and G. A. H. Wetzelaer, *Appl. Phys. Lett.*, 2016, **109**(5), 053302.

31 P. W. M. Blom, V. D. Mihailetchi, L. J. A. Koster and D. E. Markov, *Adv. Mater.*, 2007, **19**(12), 1551–1566.

32 L. Yang, J. Tumbleston, H. Zhou, H. Ade and W. You, *Energy Environ. Sci.*, 2012, 316–326.

33 C. M. Proctor, J. A. Love and T.-Q. Nguyen, *Adv. Mater.*, 2014, **26**(34), 5957–5961.

34 P. M. Beaujuge and J. M. J. Fréchet, *J. Am. Chem. Soc.*, 2011, **133**(50), 20009–20029.

35 J. A. Bartelt, Z. M. Beiley, E. T. Hoke, W. R. Mateker, J. D. Douglas, B. A. Collins, J. R. Tumbleston, K. R. Graham, A. Amassian, H. Ade, J. M. J. Fréchet, M. F. Toney and M. D. McGehee, *Adv. Energy Mater.*, 2013, **3**(3), 364–374.

36 J. H. Carpenter, A. Hunt and H. Ade, *J. Electron Spectrosc. Relat. Phenom.*, 2015, **200**, 2–14.

37 S. Mukherjee, X. Jiao and H. Ade, *Adv. Energy Mater.*, 2016, **6**(18), 1600699.

38 L. Ye, W. Zhao, S. Li, S. Mukherjee, J. H. Carpenter, O. Awartani, X. Jiao, J. Hou and H. Ade, *Adv. Energy Mater.*, 2016, 1602000.

39 S. Li, L. Ye, W. Zhao, S. Zhang, S. Mukherjee, H. Ade and J. Hou, *Adv. Mater.*, 2016, **28**, 9423–9429.

40 Y. Zhou, C. Fuentes-Hernandez, J. Shim, J. Meyer, A. J. Giordano, H. Li, P. Winget, T. Papadopoulos, H. Cheun, J. Kim, M. Fenoll, A. Dindar, W. Haske, E. Najafabadi, T. M. Khan, H. Sojoudi, S. Barlow, S. Graham, J.-L. Bredas, S. R. Marder, A. Kahn and B. Kippelen, *Science*, 2012, **336**(6079), 327–332.

41 A. Hexemer, W. Bras, J. Gossinger, E. Schaible, E. Gann, R. Kirian, A. MacDowell, M. Church, B. Rude and H. Padmore, *J. Phys.: Conf. Ser.*, 2010, **247**(1), 12007.

42 E. Gann, A. T. Young, B. A. Collins, H. Yan, J. Nasiatka, H. A. Padmore, H. Ade, A. Hexemer and C. Wang, *Rev. Sci. Instrum.*, 2012, **83**(4), 45110.

43 A. L. D. Kilcoyne, T. Tyliszczak, W. F. Steele, S. Fakra, P. Hitchcock, K. Franck, E. Anderson, B. Harteneck, E. G. Rightor, G. E. Mitchell, A. P. Hitchcock, L. Yang, T. Warwick and H. Ade, *J. Synchrotron Radiat.*, 2003, **10**, 125–136.

44 J. Ilavsky, *J. Appl. Crystallogr.*, 2012, **45**(2), 324–328.